BaI product state distribution from the reaction Ba + CF_3I

M. A. Johnson,[a] J. Allison,[b] and R. N. Zare
Department of Chemistry, Stanford University, Stanford, California 94305

(Received 7 July 1986; accepted 13 August 1986)

Under single-collision beam–gas scattering conditions the Ba + $CF_3I \rightarrow$ BaI + CF_3 reaction has been studied using laser induced fluorescence to detect the BaI $X\,^2\Sigma^+$ product. The resulting BaI $C\,^2\Pi$–$X\,^2\Sigma^+$ excitation spectrum has a complex appearance owing to the similarity of the upper and lower state rotational constants, causing a reversal in band shading, and owing to a predissociation in the upper state, causing a break off in the fluorescence of high vibrational levels in each spin-orbit subband. From the predissociation onset an upper bound of 78.5 ± 0.5 kcal/mol is placed on the BaI bond energy. The vibrational population distribution is shown to be bell shaped, peaking near $v'' = 50$, and accounts for most of the available energy. The average energy appearing in BaI rotation decreases with increasing BaI vibrational excitation. The BaI rotational distribution has a width comparable to that of the vibrational distribution.

I. INTRODUCTION

Among the earliest crossed molecular beam studies of chemical reactions are those involving an alkali atom (typically K or Rb) with an alkyl iodide molecule (CH_3I or CF_3I). These investigations demonstrated that the alkali iodide product recoiled predominantly backwards with respect to the alkali atom direction (in the center of mass frame) caused by considerable repulsive energy release during the reactive encounter.[1,2] These reactions are referred to as "impulsive" and are interpreted in the DIPR-DIP (direct interaction-product repulsion-dissociation as in photodissociation) model[3,4] as resulting in Gaussian-shaped recoil energy distributions.[5] Interest in this class of reactions has been futher heightened by the ability to orient the CH_3I or CF_3I reagent and hence to explore the influence of approach geometry on the subsequent dynamics.[6–8] Such studies have shown a strong preference for reaction at the iodine end of the alkyl iodide reagent. The alkaline earth analogs of this class of reactions, typically those involving Ba, have also received much attention. Lin, Mims, and Herm[9] (LMH) studied product translational energy distributions and found similar trends as for the alkali atoms. To obtain complementary information on the internal state distribution, Dagdigian, Cruse, and Zare[10] used laser induced fluorescence (LIF) to detect the BaI product formed in the reactions

$$\mathrm{Ba} + \mathrm{CH_3I} \rightarrow \mathrm{BaI} + \mathrm{CH_3} \tag{1}$$

and

$$\mathrm{Ba} + \mathrm{CH_2I_2} \rightarrow \mathrm{BaI} + \mathrm{CH_2I}. \tag{2}$$

They found that the BaI product vibrational distribution was inverted and approximately Gaussian in shape.

An outstanding exception to the picture that emerges for alkali and alkaline earth atom reactions with the alkyl iodides is the system

$$\mathrm{Ba} + \mathrm{CF_3I} \rightarrow \mathrm{BaI} + \mathrm{CF_3} \tag{3}$$

in which evidence has been put forward that the BaI product is formed by two reaction pathways. In the crossed molecular beam study of LMH,[9] the BaI product angular distribution shows two distinct peaks, suggesting the possibility of competing reaction channels. Unfortunately, alternative explanations involving microscopic branching could not be ruled out and the "bimodal" product distribution could have arisen as an artifact of the laboratory to center-of-mass transformation. In 1977, Smith, Whitehead, and Zare[11] (SWZ) examined this reaction using LIF detection and reported a bimodal vibrational distribution of the BaI product having two inverted distributions, one peaking at high v ($v \sim 50$), the other at low v ($v \sim 20$).

Polanyi and co-workers[12–14] have addressed the issue of bimodal distributions in reaction dynamics and they have shown that certain reactions are capable of following different trajectories over the potential surface resulting in bimodal or multimodal distributions of product internal energy states. An example of such a reaction is found in the v,T,R distributions for the reaction

$$\mathrm{Cl} + \mathrm{HI} \rightarrow \mathrm{HCl}(v,T,R) + \mathrm{I}. \tag{4}$$

In this reaction it was postulated that the bimodality in the product energy distribution was due to a geometrical effect in which attack at the H end of the HI resulted in high vibrational excitation while attack at the I end gave low vibrational excitation. Analogous examples have been reported by Breckenridge *et al.*[15] who found a clearly bimodal distribution of MgH product rotation:

$$\mathrm{Mg}(^1P_1) + \mathrm{H_2} \rightarrow \mathrm{MgH} + \mathrm{H}. \tag{5}$$

The authors postulated that the high N distribution results from Mg atom insertion while the low N distribution results from end-on attack.

These considerations suggest the possibility of a relationship between reagent approach geometry and the internal state distribution, an area of active research. Interestingly, recent work by Munakata and Kasuya[16] on the bromine analog of reaction (3):

$$\mathrm{Ba} + \mathrm{CF_3Br} \rightarrow \mathrm{BaBr} + \mathrm{CF_3} \tag{6}$$

also found evidence in the BaBr LIF spectrum for a bimodal vibrational distribution. In the latter work, the "low v" mode

[a] Present address: Department of Chemistry, Yale University, New Haven, CT 06511.
[b] Present address: Department of Chemistry, Michigan State University, East Lansing, MI 48824.

of the product energy is shown to increase with increasing reactant translational energy.

Because of the importance of reaction (3) as a prototypical example of microscopic branching, and because of the experimental possibility of controlling the collision orientation and determining the product vibration–rotation energy disposal, Bernstein and Wilcomb[5] published in 1977 a detailed analysis and comparison of the experimental results. These authors made the important observation that for the three reactions:

$$K + CH_3I \rightarrow KI + CH_3, \quad (7)$$

$$K + CF_3I \rightarrow KI + CF_3, \quad (8)$$

and

$$Ba + CH_3I \rightarrow BaI + CH_3, \quad (9)$$

the total energy appearing as product translation was consistent with the DIPR-DIP type momentum transfer constraint as discussed by Herschbach[4] and others.[3] In this model, the impulse delivered to the separating MX and CF_3 moities is governed by the energy release in the $X^- \cdots CF_3$ bond-breaking step of the harpoon mechanism postulated to control these reactions. Crudely speaking, for a given amount of energy released in this step, heavier alkyl substituents result in proportionally less translational energy release. This energy appears as internal excitation, and in the reaction series:

$$Ba + CH_3I \rightarrow BaI + CH_3,$$
$$Ba + CH_2I_2 \rightarrow BaI + CH_2I,$$
$$Ba + CHI_3 \rightarrow BaI + CHI_2,$$

the BaI LIF spectra reveal bell-shaped vibrational distributions peaking at $v'' = 15$, 40, and 62, respectively.[10,17] Moreover, Bernstein and Wilcomb[5] showed that the position and shape of the BaI vibrational distribution from Ba + CH_3I was consistent with the momentum transfer model where the BaI vibrational distribution is derived from the translational distribution via energy balance. The conclusion of their paper is that the conservation of linear momentum controls the overall energy disposal in these reactions, and that with the exception of the Ba + CF_3I reaction, this series of reactions is well-characterized both with respect to the vibrational and translational energy disposal.

Shortly after Bernstein and Wilcomb's[5] study, we reexamined the evidence of SWZ for a bimodal vibrational distribution and concluded that uncontrolled saturation effects[18] in LIF coupled with an undetected predissociation in the BaI $C\,^2\Pi_{3/2}$ state caused complexities in the spectrum which were misinterpreted as a bimodal vibrational distribution.[19] In this paper, we present the detailed analysis of the LIF spectrum and show that the vibrational distribution is actually bell shaped, in accord with other members of this reaction family. Based on higher resolution, we are also able to extract the gross form of the rotational distribution of the BaI product as a function of vibrational level. We suggest that the breadth in the rotational distribution is related to the breadth in the vibrational distribution assuming that the product recoil energy is constant.

II. EXPERIMENTAL

The results presented in this paper were all taken under so-called "beam–gas" conditions, where barium atoms from an effusive oven source are collimated into a beam and allowed to impinge on a low pressure (5×10^{-4} Torr) of CF_3I gas at room temperature. We estimate the average relative translational energy as 3 ± 1 kcal/mol. Metal atom ovens of four radically different designs and construction materials were used and found to give identical results over the range 1000–1250 K.[17] The overall intensity of the LIF spectra varied greatly, but the appearance of the spectra was unchanged. Excitation spectra were taken with a modified "folded cavity" oscillator in a nitrogen-pumped dye laser having a resolution of 0.1 cm^{-1}, continuously tunable from 5280 to 5700 Å (Coumarin dye 540 A). At this resolution, all bandhead splittings (e.g., spin-rotation) were resolved, and their positions were measured by simultaneously recording an I_2 excitation spectrum[20] with the BaI spectrum. The LIF was collected with $f/3$ optics and imaged unfiltered onto a Centronic 9283 photomultiplier tube. The spectra of the off-diagonal sequences were taken in an optically saturated regime to enhance signal to noise, while spectra used for population analysis were confirmed to be linear in laser power and photomultiplier/gated-integrator response. Spectra were obtained using a PAR 162 boxcar averager. The CF_3I reagent was obtained from PCR Research Chemicals, Inc., and subjected to freeze–pump–thaw cycles for purification. It was found that no difference in the spectra ensued when unpurified CF_3I was used directly from the bottle. Barium metal was obtained from Alpha Products and stored under oil. The oil was removed just prior to loading the oven by washing with ether.

III. RESULTS AND DISCUSSSION

A. Analysis of the BaI *C–X* spectra

As previously discussed, the excitation spectrum used by Smith, Whitehead, and Zare[11] is displayed in Fig. 1, along with the BaI vibrational population distribution extracted by these authors. In a short comment,[19] we have presented optical saturation data which showed that the "low v" feature identified by SWZ was actually the $\Delta v = -1$ sequence of a high v distribution; therefore, the evidence for vibrationally bimodality in reaction (3) must be dismissed. In this section, the peculiarities of the BaI vibrational spectroscopy which ultimately lead to this misassignment are discussed. In Fig. 2, an entire scan over the BaI $C\,^2\Pi$–$X\,^2\Sigma^+$ band is presented where the region used by SWZ has been indicated by the dashed box. It is noteworthy that the detailed bandhead structure of the two spin-orbit subbands for BaI formed by the Ba + CF_3I reaction are drastically different. The vibrational sequences in the $C\,^2\Pi_{1/2}$–$X\,^2\Sigma^+$ subband are quite regular, with an even spacing between bandheads, although there is a strong vibrational dependence to the head intensities for the two heads formed within each vibronic band. In the $C\,^2\Pi_{3/2}$–$X\,^2\Sigma^+$ subband, however, which was used for population analysis by SWZ, the bandhead structure is complicated and involves a loss of head structure around $v = 50$.

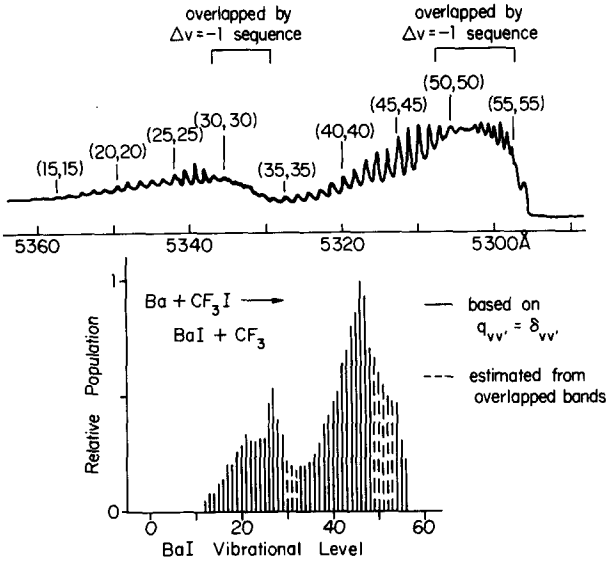

FIG. 1. Excitation spectrum and vibrational distributions of the BaI product resulting from the reaction $Ba + CF_3I \rightarrow BaI + CF_3$, as reported by Smith, Whitehead, and Zare (Ref. 11). In the upper trace, the structure on the red side of the main sequence was incorrectly identified as the $\Delta v = 0$ sequence. This actually belongs to the $\Delta v = -1$ sequence, consequently invalidating the bimodal distribution presented in the lower trace.

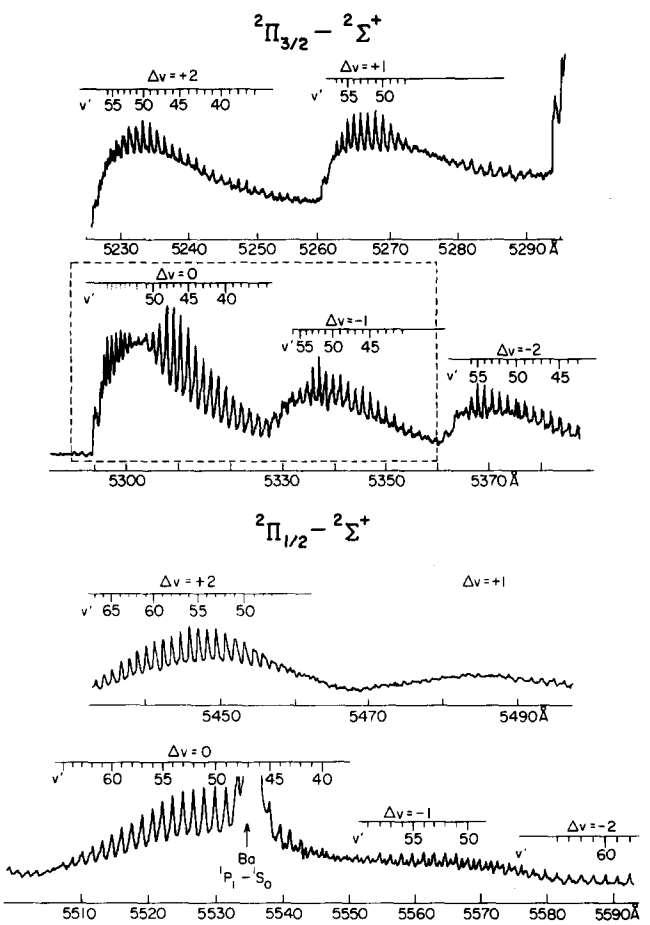

FIG. 2. BaI $C\,^2\Pi$–$X\,^2\Sigma^+$ excitation spectrum obtained from the reaction $Ba + CF_3I \rightarrow BaI + CF_3$ in this work. In this partially saturated spectrum, many $\Delta v \neq 0$ sequences are evident for both subbands. The spectrum isolated in the boxed area corresponds to the region analyzed by SWZ in Fig. 1.

In the normal rotational structure of a $^2\Pi$–$^2\Sigma$ transition, this rapid change of head structure in only one subband is atypical. It will be shown that this behavior is caused by predissociation of the $\Omega = 3/2$ component of the BaI $C\,^2\Pi$ state.

At the time the SWZ work was undertaken, an erroneous value for the BaI bond dissociation energy, $D_0^0(\mathrm{BaI}) = 102$ kcal/mol, was accepted because the role of Ba metastables in the beam–gas chemiluminescence experiments[21] had not been uncovered.[22] The more correct value of $D_0^0(\mathrm{BaI}) = 74.6 \pm 2$ kcal/mol was used by SWZ for evaluation of the reaction energetics, but these authors failed to appreciate how this value affects the stability of the BaI $C\,^2\Pi$ state. In particular, excitation of the $\Delta v = 0$ sequence at $v = 54$ results in a total of approximately 75 kcal/mol in the BaI molecule, very close to the dissociation energy to ground state atoms. The old $D_0^0(\mathrm{BaI})$ value of 102 kcal/mol would have implied that the $C\,^2\Pi$ state was still well below the energy of separated atoms at $v = 54$ and hence unable to interact with repulsive electronic states. The $\Omega = 1/2$ subband, on the other hand, lies 740 cm^{-1} below the $\Omega = 3/2$ state and can therefore support about six more vibrational levels before encountering these repulsive states at $v \sim 69$.[23] In fact, we have investigated the onset of head-loss behavior for higher vibrational levels of the $\Omega = 1/2$ state and find similar behavior to the $\Omega = 3/2$ subband, this time at $v \sim 77$ (see Fig. 3). Once again, we see that the head structure is rapidly lost as the energy of the $C\,^2\Pi_{1/2}$ state nears the energy of the separated atoms.

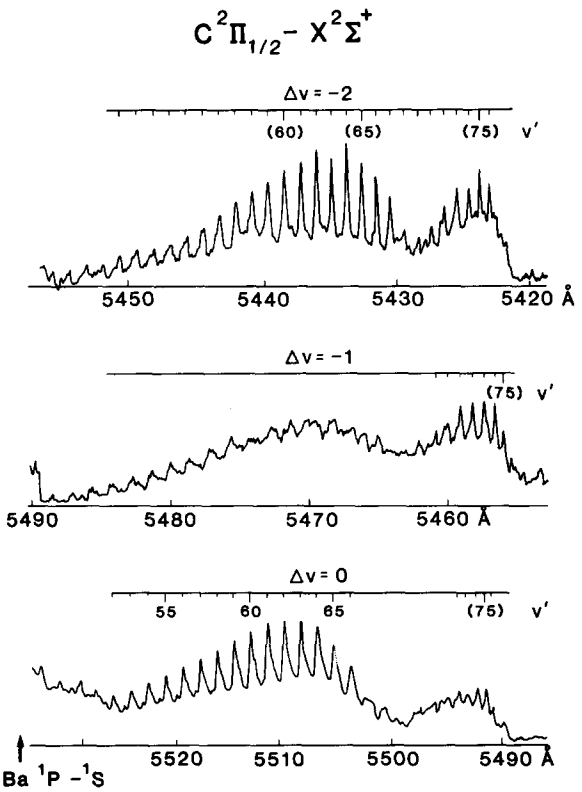

FIG. 3. BaI $C\,^2\Pi_{1/2}$–$X\,^2\Sigma^+$ excitation spectrum obtained from the reaction $Ba + CHI_3 \rightarrow BaI + CHI_2$. The v numbering for the $\Delta v \neq 0$ sequences is uncertain, as is the assignment at high v in the $\Delta v = 0$ sequence. Uncertain assignments are shown in parentheses.

Aside from the head structure of the $C\,^2\Pi_{1/2}$–$X\,^2\Sigma^+$ band, there is another interesting feature in the intensity profile. In all the vibrational sequences, vibrational levels in the range $v = 67$ to 72 are anomalously weak, where the excitation spectrum dips down and then increases in intensity above about $v = 72$. In the spectrum of both the $\Omega = 1/2$ and 3/2 components of the $C\,^2\Pi$ state, the bandheads grow closer together and finally the intensity drops precipitously at a specific v'.

To investigate further this high v behavior, we have taken extensive excitation spectra of the $C\,^2\Pi_{3/2}$–$X\,^2\Sigma^+$ system, with representative spectra shown in Fig. 4. These spectra were taken at a resolution of ~ 0.1 cm^{-1}, where the rotational contours of the vibronic sequences are clearly visible. Recall that in the branch structure of a $^2\Pi$–$^2\Sigma^+$ system, generally three bandheads are formed—two which are closely spaced and are separated by the $^2\Sigma$ state spin-rotation interaction energy $[\gamma(N + 1/2)]$, and one isolated head which is formed at about three times the rotational quantum number as that of the double head.[24] When $B' > B''$, the low J double head is formed by the Q_2 and P_{21} branch members while the high J single head is formed in the P_2 branch. When $B' < B''$, the low J double head is in the Q_{21} and R_2 branches while the high J single head is in the R_{21} branch. The heads forming the backbone of the $\Omega = 3/2$ subband are clearly seen to be doublets and are in fact lost near $v = 50$ and reappear shaded in the opposite direction above $v' = 54$. This behavior where the bandhead reverses in shading is caused by the relative magnitudes of the upper and lower state rotational constants. When $B' = B''$, no head is formed in the absence of centrifugal distortion. In fact, much of the $\Omega = 3/2$ spectrum in the region of $v' = 48$–55 is characterized by vibrational-level dependent rotational structure. Figures 5(a) and 5(b) present spectra of the $\Delta v = +2$ and $\Delta v = -2$ sequences at a resolution of about 1.0 cm^{-1}. Under high resolution (~ 0.1 cm^{-1}) it is seen that both isolated and spin-rotation-split bandheads appear and that their relative intensity changes markedly over a few vibrational levels. The brackets in Fig. 5 connect the low-J, spin-rotation split head with its corresponding high-J, isolated head. The sequences have a complex appearance because both the rotational distributions and the rotational band structure change rapidly with vibration.

The detailed explanation of the BaI $C\,^2\Pi$–$X\,^2\Sigma^+$ head structure was not possible at the time of our first report[19] of the Ba + CF_3I reaction since there were no rotationally resolved spectra available nor were spectroscopic constants

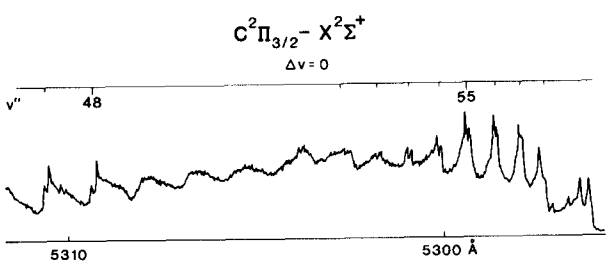

FIG. 4. Excitation spectrum of the BaI $C\,^2\Pi_{3/2}$–$X\,^2\Sigma^+$ $\Delta v = 0$ sequence band from the reaction Ba + CF_3I→BaI + CF_3. The resolution is about 0.1 cm^{-1}.

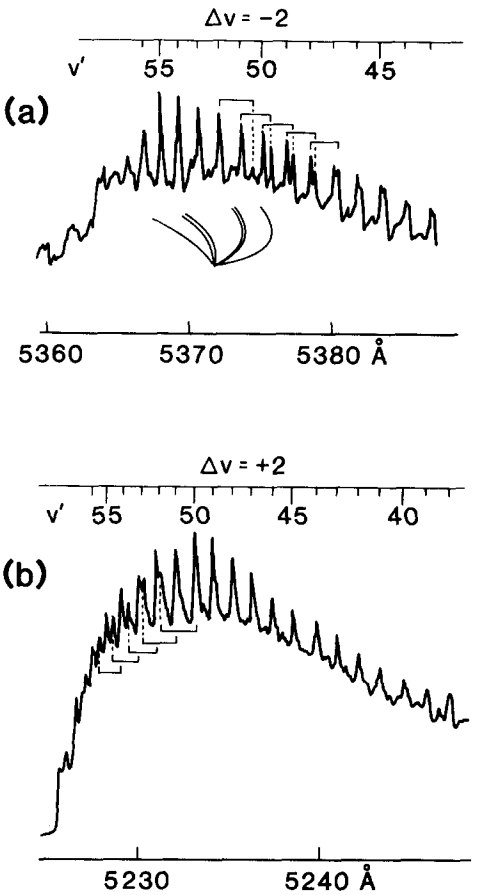

FIG. 5. Excitation spectra of the BaI $C\,^2\Pi_{3/2}$–$X\,^2\Sigma^+$ (a) $\Delta v = -2$ and (b) $\Delta v = +2$ sequences, for the reaction Ba + CF_3I→BaI + CF_3. A schematic Fortrat diagram is inset in the top trace to indicate the assignment of the heads for the (51, 53) band. The brackets connect the heads assigned to the same vibronic band.

available for any of the BaI electronic states. This situation was improved when we analyzed the C–X (0,0) band using molecular beam techniques together with optical–optical double resonance.[23,25] From these studies, we now have a complete set of rotational constants for the C and X vibrationless levels on which to build the bandhead analysis of the higher vibronic transitions. In this analysis, we have fixed the known spin-rotation splitting for the X state and lambda doubling for the C state at their $v = 0$ values. The constants B'' and D'' were allowed to vary with vibration. The vibrational dependence was modeled assuming a Morse potential for the $X\,^2\Sigma^+$ state. The B' and D' constants were determined from the measured bandhead splittings in the $\Delta v = 0$ and $\Delta v = -1$ sequences. These splittings are shown in Fig. 6 by brackets connecting the heads corresponding to a particular vibronic band. A minimum of two vibronic sequence bands are required for this analysis to obtain B' and D' uniquely. Table I presents a listing of the bandhead positions used in this analysis as well as for the $\Omega = 3/2$ bands.

The results of these fits are given in Fig. 7, which shows the vibrational dependence of the B' value for each C state component. This figure actually summarizes a great deal of information about the appearance of the BaI C–X spectrum since the relative disposition of the upper and lower state B constants determines the shading and splitting for all (v',v'')

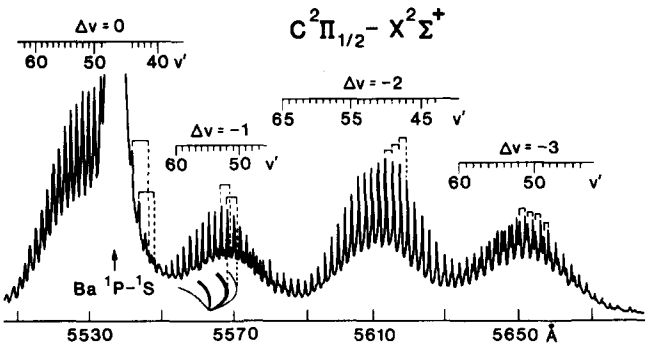

FIG. 6. Excitation spectrum of the BaI $C^2\Pi_{1/2}$–$X^2\Sigma^+$ $\Delta v = 0, -1, -2,$ and -3 sequences for the reaction Ba + $CF_3I \rightarrow$ BaI + CF_3. A schematic Fortrat diagram is inset to indicate the head assignment for the (52, 53) band. The brackets connect heads assigned to the same vibronic band.

TABLE I. Bandhead positions (cm^{-1}) for the BaI $C^2\Pi$–$X^2\Sigma^+$ system.

	$C^2\Pi_{1/2}$–$X^2\Sigma^+$	$\Delta v = 0$ sequence	
v''	P_{12}	Q_{12}	P_1
38	···	18 013.83	18 014.35
39	···	18 019.15	18 019.76
40	···	18 024.58	18 025.06
41	18 016.76	18 029.86	18 030.41
42	18 022.18	18 035.15	18 035.75
43	18 027.65	18 040.50	18 041.02
44	···	18 045.89	18 046.24
45	18 038.42	18 051.09	18 051.54
46	18 043.79	18 056.25	18 056.76
47	18 049.10	···	···
48	18 054.48	18 066.63	···
49	···	18 071.89	18 072.32
50	18 065.05	18 077.02	18 077.59
51	18 070.62	18 082.11	18 082.54
52	18 075.42	18 087.24	18 087.69
53	18 080.38	18 092.28	18 092.64
54	18 085.36	18 097.34	18 097.71
55	···	18 102.17	18 102.76
56	···	18 107.37	18 107.79
57	···	18 112.36	18 112.71
58	···	18 117.29	18 117.71
59	···	18 122.27	18 122.74
60	···	18 127.00	18 127.47
61	···	18 131.92	18 132.37
62	···	18 136.71	18 137.08

	$C^2\Pi_{1/2}$–$X^2\Sigma^+$	$\Delta v = -1$ sequence	
v''	P_{12}	Q_{12}	P_1
46	···	17 924.91	17 924.91
47	17 922.19	17 930.74	17 930.74
48	17 927.85	17 936.20	17 936.52
49	17 933.51	17 941.86	17 942.07
50	17 939.18	17 947.40	17 947.66
51	17 944.81	17 953.02	17 953.21
52	17 950.39	17 958.50	17 958.76
53	17 956.05	17 963.96	17 964.21
54	17 961.60	17 969.55	17 969.80
55	17 967.22	17 974.94	17 975.25
56	17 972.63	17 980.41	17 980.59
57	17 978.12	17 985.77	17 985.94
58	17 983.68	17 991.24	17 991.45
59	17 989.08	17 996.62	17 996.82
60	17 994.41	18 001.97	18 002.40
61	17 998.87	18 007.33	18 007.48
62	···	18 012.62	18 012.81
63	···	18 017.84	18 018.08
64	···	18 023.00	18 023.18
65	···	18 028.18	18 028.36

TABLE I. (*continued*).

	$C^2\Pi_{3/2}$–$X^2\Sigma^+$	$\Delta v = -2$ sequence
v''	P_2	$P_{21} + Q_2$
46	···	18 554.44
47	18 553.60	18 560.22
48	18 559.68	18 566.48
49	18 565.62	18 572.39
50	18 571.51	18 578.51
51	18 577.37	18 584.32
52	18 582.92	18 590.13
53	18 588.34	18 595.72
54	18 593.53	18 601.72
55	···	18 606.53
56	···	18 611.60
57	···	18 616.24
58	···	18 620.17

	$C^2\Pi_{3/2}$–$X^2\Sigma^+$	$\Delta v = 0$ sequence
v''	P_{21}	Q_2
40	18 787.52	···
41	18 793.03	···
42	18 798.32	···
43	18 803.61	18 804.08
44	18 808.98	18 809.45
45	18 813.92	18 814.36
46	18 819.08	18 819.57
47	18 824.01	18 824.47
48	18 828.77	18 829.26
49	···	···
50	···	···
51	···	···
52	···	···
53	···	···
54	18 865.46	···
55	18 868.27	···
56	18 871.12	···
57	18 873.49	···
58	18 875.42	···

	$C^2\Pi_{3/2}$–$X^2\Sigma^+$	$\Delta v = 2$ sequence	
v''	Q_{21}	R_2	R_{21}
45	19 086.35	19 086.59	19 094.47
46	19 090.36	19 090.58	19 097.75
47	19 094.20	19 094.40	19 101.21
48	19 097.89	19 098.14	19 104.53
49	19 101.79	19 102.01	19 107.92
50	19 105.56	19 105.80	19 110.94
51	19 108.98	···	19 113.83
52	19 112.21	···	19 116.63
53	19 115.14	···	19 119.21
54	19 117.88	···	19 121.53
55	19 119.97	···	···
56	19 124.05	···	···

bands as well as indicates whether a head exists or not for a given (v',v'') sequence member. As an example, the crossing of the B' and B'' curves at approximately $v'' = 15$ has not been recognized previously. It is now apparent that both subbands will have a headless region around $v = 15$ in the $\Delta v = 0$ sequence, with heads degraded to the red below $v = 15$ and to the blue above $v = 15$. This fact implies that previous vibrational assignments are actually incorrect since a simple counting of the "bumps" through the headless region results in skipping over vibrational levels. In the BaI

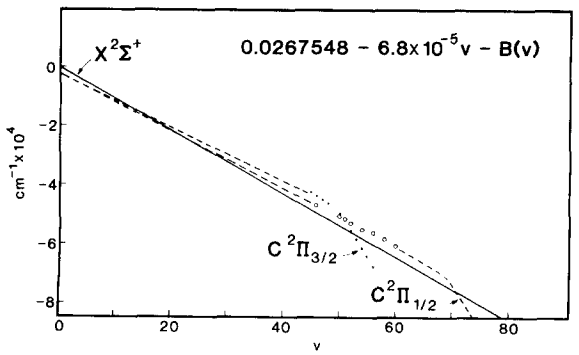

FIG. 7. Vibrational dependence of the X and C state rotational constants obtained from fits to head splittings. Dashed lines indicate interpolated regions.

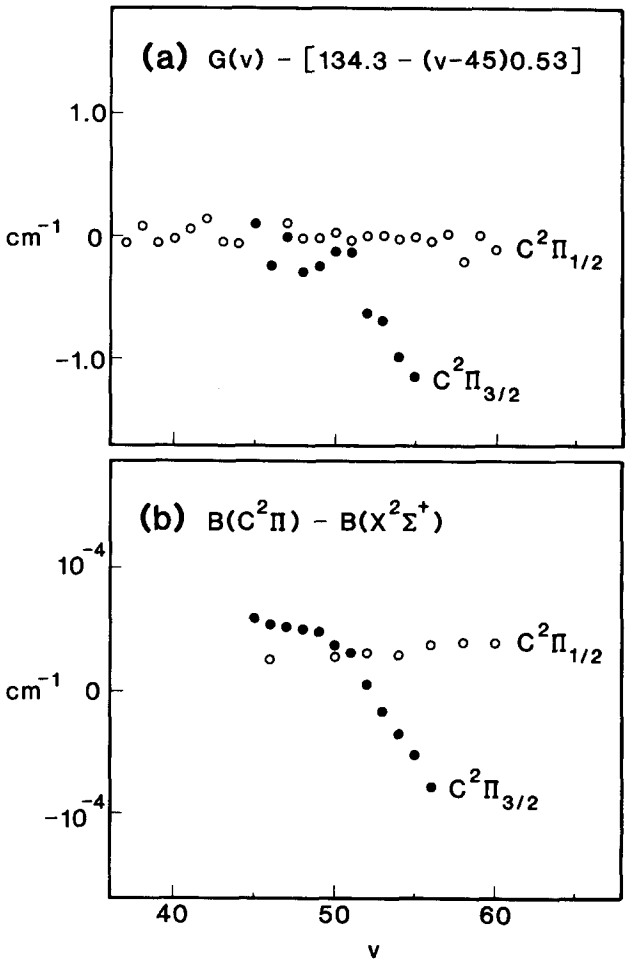

FIG. 8. (a) Vibrational dependence of the vibrational spacing $\Delta G(v) = E(v+1) - E(v)$ for the $\Omega = 1/2$ and 3/2 components of the BaI $C\,^2\Pi$ state. (b) Vibrational dependence of the effective rotational constants for the $\Omega = 1/2$ and 3/2 components of the BaI $C\,^2\Pi$ state.

C–X system, the spacing between the heads in the $\Delta v = 0$ sequences is nearly the same as the displacement of the head from the vibronic origin. Hence, previous assignments above $v = 15$ in the $\Delta v = 0$ sequence must be increased by two vibrational quanta. This counting correction also applies to the head reversal in the $\Omega = 3/2$ subband near $v' = 52$. High resolution spectroscopy was required to establish even the vibrational numbering for the C–X band system in this molecule. Interestingly, SWZ reexamined the BaI $\Delta v = 0$ excitation spectrum for the Ba + CH_3I reaction and argued for a possible bimodality in the vibrational distribution, where levels $v'' = 0$–40 are populated. The "bimodal" feature in this spectrum coincides with the vibrational levels around $v = 24$—those levels where the heads are just reforming according to Fig. 7. Therefore this vibrational product distribution is also likely bell shaped. In this regard, it is important to bear in mind the subtleties of the underlying rotational structure of the vibrational spectra even if only a crude distribution of product vibrational energy is desired.

B. Evidence for predissociation in the BaI C state

We summarize here the evidence for identification of a perturbation in the $C\,^2\Pi$ state as a predissociation rather than a simple formation of a vibrational head of heads.[24] In Fig. 8 the rotational constant and vibrational origin spacing of the C state spin-orbit components are shown as a function of vibrational level. In both $B(v)$ and $\Delta G(v)$ plots, a sharp drop-off occurs at approximately $v = 50$, as expected when a potential curve is distorting rapidly at the outer wall. The observed spread of v over which this drop-off occurs is, however, quite wide (about eight vibrational levels) indicating that the matrix element for the interaction must be large (200–500 cm^{-1}). Also, note that the nature of the perturbation is such that the $\Omega = 3/2$ and $\Omega = 1/2$ states are not equally perturbed. This indicates that $\Delta\Omega = 0$ crossings are favored, possibly implying a Hund's case (c) coupling for these states at large internuclear distances. Note that the distortion of the potential in the $\Omega = 3/2$ state accounts for the rapidly increasing Franck–Condon factor for the $\Delta v \neq 0$ sequences with increasing vibration, and that the Ba + CF_3I reaction produces a high level of vibrational excitation. The rapid change in the $\Delta G(v)$ vs v plot for the $\Omega = 3/2$ component accounts for the compressed appearance of the heads at high v in the $\Omega = 3/2$ subband (see Fig. 2).

It remains to be determined whether the sharp falloff in the $\Delta v = 0$ spectrum at $v = 62$ arises because of a vibrational head of heads or because of predissociation. To settle this point, we obtained BaI excitation spectra from the Ba + $CHI_3 \rightarrow$ BaI + CHI_2 reaction which creates an even more highly excited vibrational distribution, $v'' = 50$ to 80 (see Fig. 3). Spectra of the $\Delta v = +2$ and $\Delta v = 0$ sequences of the $\Omega = 3/2$ subband are presented in Fig. 9, which show no additional features arising from higher vibrational levels. Consequently we conclude that the drastic drop in fluorescence intensity results from a predissociation of the $C\,^2\Pi$ state at $v \sim 62$ in the $\Omega = 3/2$ component and at $v \sim 78$ in the $\Omega = 1/2$ component (see Fig. 3).

Inspection of Fig. 3 shows a dip in the fluorescence intensity near $v' \approx 70$ in the $\Omega = 1/2$ subband for the $\Delta v = 0,1,2$ sequences. This occurs at the same region where the $\Omega = 3/2$ component is completely predissociated. It is interesting to speculate that this effect may arise from interaction with the same repulsive states. If indeed the $\Omega = 3/2$ and 1/2 components share a common perturber, then this suggests the perturbation is a repulsive $^2\Pi$ state with an in-

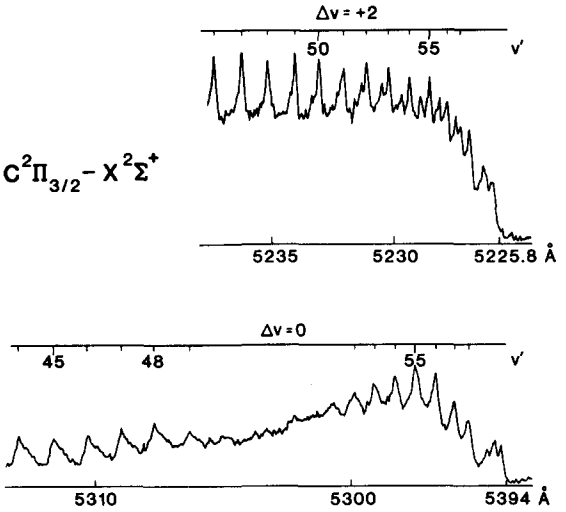

FIG. 9. Excitation spectra of the BaI $C\,^2\Pi_{3/2}$–$X\,^2\Sigma^+$ $\Delta v = 0$ and $\Delta v = +2$ sequences from the reaction Ba + CHI_3→BaI + CHI_2.

verted spin-orbit ordering similar in magnitude to the spin-orbit splitting in the C state.

The presence of the predissociation in the C state sets an upper bound on the D_0^0(BaI) bond energy of 78.5 ± 0.5 kcal/mol, which is somewhat higher than presently accepted values ($\sim$73 kcal/mol).[22,26] This bound is based on the onset of the predissociation in the $C\,^2\Pi_{3/2}$ component after the (62, 62) band at 18 881 cm^{-1} using the ground state vibrational constants from Ref. 10. The error estimate is based on the uncertainty in numbering of the last vibrational bandhead due to the irregular bandhead structure after $v'' = 58$. Figure 10 presents a schematic set of potential curves indicating the likely shape of the $C\,^2\Pi$ state potential.

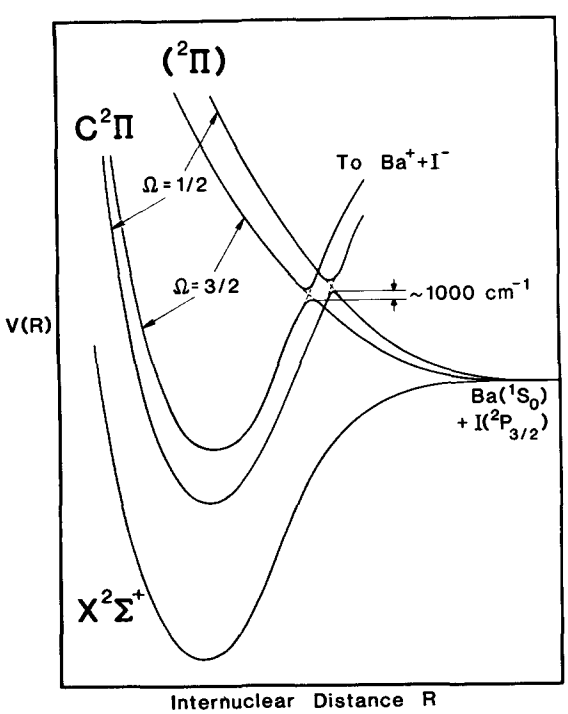

FIG. 10. Schematic potential curves for the BaI X and C states.

C. Extraction of the BaI vibrational population distributions

The vibrational population analysis is based on the $\Delta v = 0$ sequence, recorded in a regime in which the intensity varies linearly with laser power. The $\Omega = 1/2$ subband is used for most v's since this component of the upper state is predissociated at v' levels not populated in the Ba + CF_3I reaction. For the $\Delta v = 0$ sequence, the Franck–Condon factor is assumed to be essentially unity. The presence of the $Ba\,^1P_1$–$^1S_0$ resonance line obscures the $\Delta v = 0$ sequence near $v' = 47$. Consequently for $v' \lesssim 45$ the $\Omega = 3/2$ subband is used. Because the relative intensities of the high J and low J heads vary with v, it is necessary to correct bandhead intensities for changing rotational distributions.

At a first glance (see Fig. 6) the $\Delta v = -2$ sequence appears to be very simple and isolated. A more detailed analysis shows, however, that the heads in this sequence result from a chance overlap of the bandheads among nearest vibronic members, so that this band is not suitable for population analysis. The $\Delta v = +1$ sequence (see Fig. 2) does not form a head at the rotational levels generated in the reaction and the $\Delta v = +2$ sequence forms well populated heads, but is badly overlapped by the $\Delta v = -4$ sequence of the $\Omega = 3/2$ subband. The $\Delta v = -1$ sequence of the $\Omega = 1/2$ subband is suitable for population analysis, but the effect of the vibration-dependent rotational bandhead structure is severe for this sequence (see Fig. 11) and had to be taken into account.

Our strategy is to use the bandhead intensities in the $\Delta v = 0$ and $\Delta v = -1$ sequences to establish the form of the rotational distributions and then to use these distributions to extract the vibrational distribution from the bandhead intensities in the $\Delta v = 0$ sequence.

To determine the vibrational dependence of the rotational distribution, the intensities of the high-J and low-J heads were fit by a convolution program simulating the $\Delta v = 0$ and $\Delta v = -1$ sequences for a given v'' level. The rotational distribution was then adjusted to achieve reasonable agreement. The high-J head dominates the $\Delta v = -1$ spectrum for $v'' < 54$, as shown in Fig. 11. A fit could be obtained with a Gaussian form for the J distribution:

$$P(v,J) = (2J+1)\exp\{-(F_J - F_v)^2/\sigma_v^2\}, \qquad (10)$$

where F_J is the fraction of the total available energy appearing in rotation. The total energy available was taken as 12 000 cm^{-1}. The parameters F_v and σ_v describe the vibrational dependence of the rotational distributions and were adjusted for each v. F_v and σ_v were varied until the rotational distributions given by Eq. (10) give the observed ratio of bandhead intensities for the $\Delta v = 0$ and $\Delta v = -1$ sequences of the $C\,^2\Pi_{1/2}$–$X\,^2\Sigma^+$ subband. Two sequences are used in the fit since J values where the two main bandheads form in each vibronic band (i.e., in the $Q_{12} + P_1$ and P_{12} branches) vary strongly with vibrational sequence (see Table II). This procedure significantly constrains the form of the rotational distributions since four ranges of J are sampled from $J = 140$ to $J = 370$ using the two heads in two sequences. The values of F_v and σ_v which reproduce the

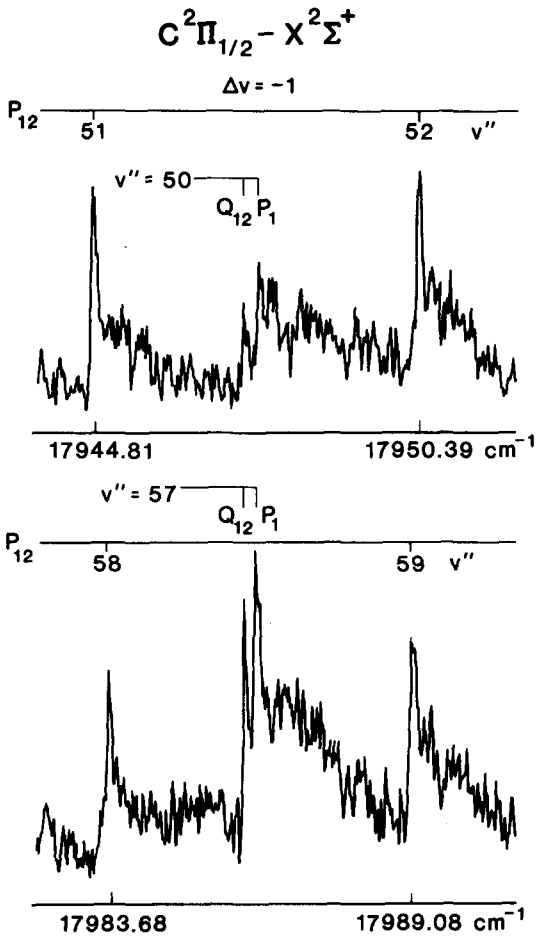

FIG. 11. Excitation spectra of the BaI $C\,^2\Pi_{1/2}$–$X\,^2\Sigma^+$ $\Delta v = -1$ sequence at a resolution of 0.1 cm^{-1} displaying the relative intensities of the P_{12} "high-J" head and the $Q_{12}+P_1$ "low-J" heads around $v''=50$ and $v''=57$.

bandhead intensities are given by the following empirically determined formulas:

$$F_v = 0.125 - 0.0085(v-50) \tag{11}$$

and

$$\sigma_v = 0.46 - 0.010\,75v + 7.5\times10^{-5}v^2. \tag{12}$$

Figure 12 displays the resulting rotational distributions for three vibrational levels, $v''=40$, 50, and 60. It is seen that increasing vibrational excitation of the product is correlated with decreasing rotational excitation. It is also apparent that

TABLE II. Vibrational sequence dependence of the rotational bandheads in the BaI $C\,^2\Pi_{1/2}$–$X\,^2\Sigma^+$ subband ($v''=50$).

Rotational branch	Vibrational sequence	J at head
$Q_{12}+P_1$	0	250
P_{12}	0	370
Q_{12}	−1	140
P_{12}	−1	280

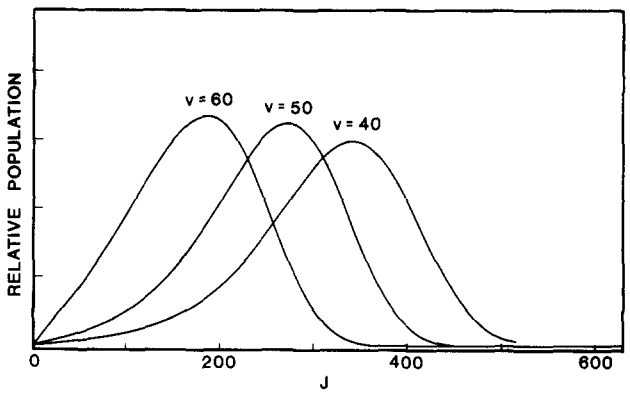

FIG. 12. Rotational distributions for the BaI $X\,^2\Sigma^+$ product obtained by fitting bandhead intensities for BaI $C\,^2\Pi$–$X\,^2\Sigma^+$ from the reaction Ba + CF_3I→BaI + CF_3.

the width of the rotational distribution increases proportionally to the most probable J value. These rotational distributions should be regarded as first-order estimates rather than a rigorous fit to contours. These distributions are introduced here primarily to correct the vibrational distributions for changes in the rotational distribution. In fact while the rotational distributions shown in Fig. 12 do reproduce the intensities of the bandheads, they systematically underestimate the population at low J, away from the heads. Consequently, we are hesitant to make firmer conclusions about the rotational energy disposal. In particular, we are unable to rule out more complex rotational distributions such as bimodal ones.

The rotationally corrected vibrational distribution for the reaction Ba + CF_3I→BaI + CF_3 is shown in Fig. 13. It has the expected bell-shaped appearance seen previously for reactions of barium with alkyl halides, except the reaction Ba + CF_3Br. Naaman[27] has suggested that this remaining anomaly might be caused by unrecognized CF_3Br dimers in the seeded reactant beam used by Munakata and Kasuya.[16] In Naaman's study of Ba + $(CF_3I)_2$, the BaI product is formed in much lower vibrational states than the reaction with monomer. Under our conditions (ambient low-pressure CF_3I gas) the dimer concentration is negligible. Munakata and Kasuya have considered this possibility,[28] and they

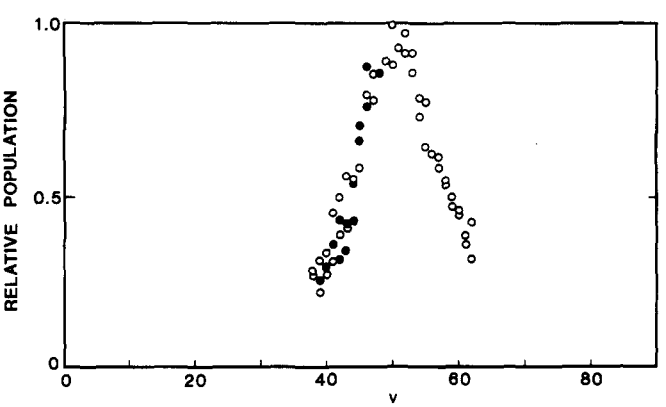

FIG. 13. Vibrational distribution for the BaI $X\,^2\Sigma^+$ product produced in the reaction Ba + CF_3I→BaI + CF_3. Open circles indicate data obtained from the $C\,^2\Pi_{1/2}$–$X\,^2\Sigma^+$ subband. Closed circles indicate data obtained from the $C\,^2\Pi_{3/2}$–$X\,^2\Sigma^+$ subband.

argue against the presence of dimers based on mass spectrometric identification of their beam species.

In the light of these results, it is of interest to reexamine the circumstances that lead SWZ to conclude that the Ba + CF_3I reaction yielded a BaI bimodal vibrational distribution. The Ba + CF_3I reaction produces BaI with more vibrational excitation than had been previously seen in studies of Ba + HI,[29] and Ba + CH_3I and CH_2I_2.[10] Smith, Whitehead, and Zare[11] were thus faced with a much bigger contribution to the LIF spectrum from the $\Delta v = -1$ sequence than occurs for a distribution peaking just ten vibrational levels lower (i.e., from Ba + CH_2I_2). The $\Delta v = -1$ spectrum overlaps the region in which the low-v portion of the $\Delta v = 0$ sequence would appear as an isolated feature. This accounts for the misassignment by SWZ of the $\Delta v = -1$ sequence as belonging to $\Delta v = 0$. It is worth emphasizing that in the present study the capability of resolving the spin-rotation doublet in the head structure was invaluable in producing unambiguous sequence assignments. Because the J values at which the bandheads occur are strongly dependent on vibrational sequence, even in highly congested regions of the spectrum, the sequence identity of a given bandhead feature is readily established. In this way, we can conclusively state that the $\Delta v = -1$ feature of both subbands are not contaminated by low-v members of the $\Delta v = 0$ sequence.

Figure 14 displays a typical region in the $\Delta v = -1$ sequence at the $C\,^2\Pi_{1/2}$–$X\,^2\Sigma^+$ subband at a laser bandwidth of 0.1 cm^{-1}. The heads corresponding to the $\Delta v = 0$ sequence bands at low v are easily distinguishable from $\Delta v = -1$ members at high v since the spin-rotation splitting is much more pronounced for the $\Delta v = 0$ bands. Additionally, the high-J heads are evident by their single-headed character. These results confirm our earlier suggestion that this was the case,[19] in which we used optical saturation to probe relative Franck–Condon factors for the vibronic features and hence distinguish between $\Delta v = 0$ and $\Delta v = -1$ sequences. With the present understanding of the bandhead structure of the BaI C–X band system, we can actually make a more powerful statement about possible low-v contributions to the spectrum. An albeit unlikely suggestion may be

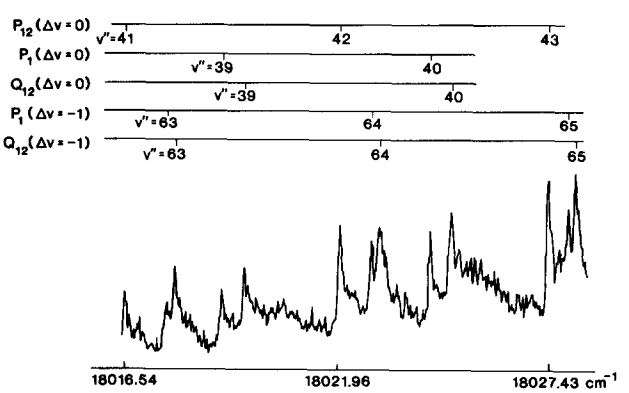

FIG. 14. High resolution scan of the overlapping $\Delta v = 0$ and $\Delta v = -1$ sequences of the BaI $C\,^2\Pi_{1/2}$–$X\,^2\Sigma^+$ subband from the reaction Ba + CF_3I → Ba + CF_3. The bandhead splittings uniquely identify the sequence assignment of vibronic features. The $\Delta v = -1$ members are shaded so that they can be more readily distinguished from the $\Delta v = 0$ members.

forwarded the low-v BaI molecules are produced with a very high degree of rotational excitation. If we focus on the $\Delta v = +1$ sequence of the $\Omega = 1/2$ subband (see Fig. 2), we find that $B' \sim B''$ for many v's around 25 (the "low-v mode"), so that bandheads will form at very high J. We find none of these heads populated and conclude that the BaI C–X spectrum yields no evidence for anything other than a single, bell-shaped distribution of vibrational energy from the reaction Ba + $CF_3I \rightarrow$ BaI + CF_3.

D. The Ba + CF_3I reaction dynamics

Until the BaI bond energy is more firmly established,[30] we are unable to make quantitative statements on the energy partitioning for this reaction. Nevertheless, it is clear that the available energy ΔE for product excitation is in the range $24 < \Delta E < 30$ kcal/mol. The peak in the vibrational distribution corresponds to ~19.9 kcal/mol, indicating the BaI vibrational excitation is the major channel for energy disposal.

Note that the fits to the rotational distributions presented in Sec. III C required a total available energy of 34 kcal/mol, indicating that a significant portion of the rotational energy must arise from the collision energy. At the most probable product vibration, $v'' = 50$, the most probable J'' value is about 270 (see Fig. 12) corresponding to a rotational energy of about 5 kcal/mol. Based on the DIPR-DIP model,[31] the most probable translational energy is $\sim 5.7 \pm 2.3$ kcal/mol, which is comparable to the rotational energy. Hence the sum of the energy in product translation, BaI vibration and BaI rotation seems to account for nearly all available energy, suggesting that the CF_3 product has little internal energy. Geometrical arguments support this inference since the structure of CF_3 is pyramidal and the electron-jump reaction mechanism is not expected to exert a torque on the departing CF_3 fragment.

Conservation of angular momentum implies that the BaI rotation arises from the orbital angular momentum of the reagents. Furthermore, the width of the rotational distribution (~5.4 kcal/mol) closely matches the width of the vibrational distribution (~5.1 kcal/mol). This last observation, combined with a model[32] in which the product recoil energy is assumed constant, suggests that the width of the BaI vibrational distribution may be a consequence of the dynamics of the Ba + CF_3I reaction, i.e., the reaction probability as a function of translational energy and impact parameter. This picture should be contrasted with the model[4,5] where the width is assumed to mirror only the photodissociation recoil distribution. If BaI rotation plays an important role in determining the BaI vibrational distribution, then experiments with velocity selected reagents are necessary to elucidate more deeply the reaction dynamics.

ACKNOWLEDGMENTS

This work is supported in part by the Air Force Office of Scientific Research under AFOSR F49620-86-C-0016 and by the National Science Foundation under NSF CHE 85-05926.

[1]D. R. Herschbach, G. H. Kwei, and J. A. Norris, J. Chem. Phys. **34**, 1842 (1961).
[2]A. M. Rulis, B. E. Wilcomb, and R. B. Bernstein, J. Chem. Phys. **60**, 2822 (1974).
[3]P. J. Kuntz, M. H. Mok, and J. C. Polanyi, J. Chem. Phys. **50**, 4623 (1969).
[4]D. R. Herschbach, Faraday Discuss. Chem. Soc. **55**, 233 (1973).
[5]R. B. Bernstein and B. E. Wilcomb, J. Chem. Phys. **67**, 5809 (1977).
[6]P. R. Brooks and E. M. Jones, J. Chem. Phys. **45**, 3449 (1966).
[7]R. J. Beuhler and R. B. Bernstein, Chem. Phys. Lett. **2**, 166 (1968).
[8]P. R. Brooks, Faraday Discuss. Chem. Soc. **55**, 299 (1973).
[9]S.-M. Lin, C. A. Mims, and R. R. Herm, J. Phys. Chem. **77**, 569 (1973).
[10]P. J. Dagdigan, H. W. Cruse, and R. N. Zare, Chem. Phys. **15**, 249 (1976).
[11]G. P. Smith, J. C. Whitehead, and R. N. Zare, J. Chem. Phys. **67**, 4912 (1977).
[12]H. Heydtmann and J. C. Polanyi, Appl. Opt. **10**, 1738 (1971).
[13]L. T. Cowley, D. S. Horne, and J. C. Polanyi, Chem. Phys. Lett. **12**, 144 (1972).
[14]M. A. Nazar, J. C. Polanyi, and W. J. Skrlac, Chem. Phys. Lett. **29**, 473 (1974).
[15]W. H. Breckenridge and H. Umemoto, J. Chem. Phys. **80**, 4168 (1984); **81**, 3852 (1984).
[16]T. Munakata and T. Kasuya, J. Chem. Phys. **81**, 5608 (1984).
[17]M. A. Johnson, Ph.D. thesis, Stanford University, Stanford, California, 1983.
[18]R. I. Altkorn and R. N. Zare, Annu. Rev. Phys. Chem. **35**, 265 (1984).
[19]J. Allison, M. A. Johnson, and R. N. Zare, Faraday Discuss. Chem. Soc. **67**, 124 (1979).
[20]S. Gerstenkorn and P. Luc, *Atlas de Spectre d'Absorption de la Molecule d'Iode* (CNRS, Paris, 1978).
[21]C. R. Dickson, J. B. Kinney, and R. N. Zare, Chem. Phys. **15**, 243 (1978).
[22]R. C. Estler and R. N. Zare, Chem. Phys. **28**, 253 (1978).
[23]M. A. Johnson, C. Noda, J. S. McKillop, and R. N. Zare, Can. J. Phys. **62**, 1467 (1984).
[24]G. Herzberg *Spectra of Diatomic Molecules*, 2nd ed. (Van Nostrand, New York, 1950).
[25]M. A. Johnson, C. R. Webster, and R. N. Zare, J. Chem. Phys. **75**, 5575 (1981).
[26]P. D. Kleinschmidt and D. L. Hildenbrand, J. Chem. Phys. **68**, 2819 (1978).
[27]R. Naaman (private communication); Laser Chem. **5**, 385 (1986).
[28]T. Munakata and T. Kasuya (private communication).
[29]H. W. Cruse, P. J. Dagdigian, and R. N. Zare, Faraday Discuss. Chem. Soc. **55**, 277 (1973).
[30]C. Noda, J. S. McKillop, M. A. Johnson, J. Waldeck, and R. N. Zare, J. Chem. Phys. **85**, 856 (1986).
[31]This estimate is based on the relation $E'_{\text{trans}}(\text{BaI}) = P^2(\text{BaI})/2\mu(\text{BaI}, CF_3)$, where $P(\text{BaI})$ is the center of mass momentum and $\mu(\text{BaI}, CF_3)$ is the reduced mass of BaI and CF_3 (see Ref. 5). In the DIPR-DIP, $P(\text{BaI}) = P(\text{KI})$ from the reaction $K + CF_3I \rightarrow KI + CF_3$ and $P(\text{KI})$ is taken from Ref. 5 to be 12.9 Å^{-1}. The error estimate represents the spread in $C\text{–}I^-$ energy release for the reactions $Ba + CH_3I$ and $K + CH_3I$.
[32]C. Noda and R. N. Zare, J. Chem. Phys. (submitted).